RSC Advances

PAPER

View Article Online
View Journal | View Issue

Cite this: *RSC Adv.*, 2017, **7**, 23699

Highly efficient photocatalytic degradation of methylene blue by P2ABSA-modified TiO_2 nanocomposite due to the photosensitization synergetic effect of TiO_2 and P2ABSA

Chuanxi Yang,[ab] Wenping Dong,[c] Guanwei Cui,[d] Yingqiang Zhao,[d] Xifeng Shi,[d] Xinyuan Xia,[d] Bo Tang *[d] and Weiliang Wang *[ae]

Received 27th February 2017
Accepted 16th April 2017

DOI: 10.1039/c7ra02423a

rsc.li/rsc-advances

To enhance the photocatalytic activity of TiO_2, poly-2-aminobenzene sulfonic acid (P2ABSA)-modified TiO_2 nanocomposites were successfully synthesized using an *in situ* oxidative polymerization method. The modified nanocomposites were characterized by scanning electron microscopy, X-ray diffraction, transmission electron microscopy, X-ray photoelectron spectroscopy, UV-vis diffuse reflectance spectroscopy, and a photocurrent test. The photocatalytic degradation of methylene blue was chosen as a model reaction to evaluate the photocatalytic activities of TiO_2 and P2ABSA/TiO_2 nanocomposites, with results indicating that P2ABSA/TiO_2 exhibited the higher activity. The apparent first-order rate constant, k_{app}, of P/T(2/1) was 0.0138 min^{-1}, which was six times higher than that of TiO_2 (0.0021 min^{-1}). Meanwhile, the P2ABSA/TiO_2 nanocomposites showed excellent photocatalytic stability, which was dependent on structural stability. A photocatalytic activity enhanced mechanism has been proposed, accounting for the photosensitization effect and synergetic effect of TiO_2 with P2ABSA. Mass spectroscopy analysis showed that there were two possible degradation pathways for MB, *via* degradation of the chromophoric group or the auxochrome group.

1. Introduction

Semiconductor TiO_2 is an excellent photocatalyst owing to its good photocatalytic activity and stability.[1,2] However, the wide band gap (3.2 eV) of TiO_2 limits its visible light utilization, while its low quantum efficiency (<20%) restricts electron–hole separation, which generates reactive oxygen species (ROS) to degrade organic pollutants.[3,4] Many approaches, such as metal/nonmetal doping, noble metal deposition, and dye sensitization, have been attempted to enhance the photocatalytic performance of TiO_2 by improving its photoresponse and quantum efficiency.[5–7]

Recently, conducting polymers, such as polyaniline (PANI), polythiophene (PTh), poly-*o*-phenylenediamine (PoPD), and their derivatives, have been reported as promising modifiers for TiO_2 photocatalysts.[8] The modification of TiO_2 with conducting polymers has been explored to extend its visible light response owing to the photosensitization effect between TiO_2 and the conducting polymer.[9] For example, Pandi Muthirulan *et al.* reported that PoPD/TiO_2 nanocomposites showed high photocatalytic activity in the photodegradation of rhodamine B owing to the photosensitization effect.[10] This modification also enhanced the photocatalytic activity owing to the synergetic effect between TiO_2 and the conducting polymer. Zhang *et al.* reported that PANI/TiO_2 nanocomposites exhibited excellent photocatalytic performance in the degradations of methylene blue and rhodamine B owing to the synergetic effect between TiO_2 and PANI.[11]

In addition to PANI and PoPD, poly-2-aminobenzene sulfonic acid (P2ABSA) has also been applied to conducting polymer-modified TiO_2 to improve its photocatalytic performance.[12] As a typical conducting polymer, P2ABSA has attracted considerable attention since its discovery. Taking advantage of its unique electrical, optical, and photoelectric properties, the combination of P2ABSA with TiO_2 was expected to induce an interesting charge transfer to enhance the photocatalytic activity of TiO_2 under visible light irradiation.[13] However, this photocatalytic activity enhanced mechanism has not been

[a]College of Geography and Environment, Shandong Normal University, Jinan 250014, P. R. China. E-mail: sdqcsdnu@163.com; Fax: +86 531-8618-0017; +86 531-8618-2550
[b]College of Resources and Environmental Sciences, China Agricultural University, Beijing 100193, P. R. China
[c]Shandong Academy of Environmental Science and Environmental Engineering Co, Ltd, Jinan 250013, P. R. China
[d]College of Chemistry, Chemical Engineering and Materials Science, Collaborative Innovation Center of Functionalized Probes for Chemical Imaging in Universities of Shandong, Key Laboratory of Molecular and Nano Probes, Ministry of Education, Shandong Provincial Key Laboratory of Clean Production of Fine Chemicals, Shandong Normal University, Jinan 250014, P. R. China. E-mail: tangb@sdnu.edu.cn
[e]Institute of Environment and Ecology, Shandong Normal University, Jinan 250014, P. R. China

studied.[14] The photocatalytic process of P2ABSA/TiO_2 involves a primary reaction that generates holes and electrons, and a secondary reaction that generates ROS.[15] Therefore, successfully establishing a quantitative estimate of the contributions of P2ABSA in these primary and secondary reactions is important.

About 15% of total global dye production is lost during the dyeing process and released in textile effluents.[16] The release of those colored waste waters into the ecosystem is a substantial source of non-aesthetic pollution, eutrophication, and perturbation in aquatic life.[17] The photocatalytic degradation of methylene blue (MB), a typical conjugated aromatic dye, was chosen as a model reaction to evaluate photocatalyst activities due to the obvious change to blue during photocatalytic degradation.[18] Meanwhile, identifying the intermediate products and degradation pathways of MB is also an important part of the photocatalytic activity test and photocatalytic mechanism. The main dispute regarding MB degradation is between degradation of the central aromatic ring, as reported by Ammar Houas, and degradation of the methyl substituent on the ambilateral benzene ring, as reported by Muhammad A. Rauf.[19,20] However, many different degradation pathways for MB have also been reported by Zhou Lincheng,[21] Ma Junjun,[23] and Castro.[22] Therefore, it is important to identify the intermediate products and propose possible MB degradation pathways during the photocatalytic reaction process.

In our studies, P2ABSA/TiO_2 nanocomposites were synthesized using an *in situ* oxidative polymerization method. The modified photocatalysts were characterized by scanning electron microscopy (SEM), X-ray diffraction (XRD), transmission electron microscopy (TEM), X-ray photoelectron spectroscopy (XPS), ultraviolet-visible diffuse reflectance spectroscopy (UV-vis DRS), and a photocurrent test. The results indicated that P2ABSA was present on the TiO_2 surface, and did not impact the lattice structure and grain size of TiO_2. The presence of P2ABSA enhanced the visible light response and photoelectric performance. The photocatalytic degradation of MB was chosen as a model reaction to evaluate the photocatalytic activities of TiO_2 and P2ABSA/TiO_2 nanocomposites. The results indicated that the P2ABSA/TiO_2 nanocomposites exhibited higher activities. The apparent first-order rate constant, k_{app}, for a P2ABSA/TiO_2 ratio of 2 : 1 was 0.0138 min^{-1}, which was six times higher than that of TiO_2 (0.0021 min^{-1}). Meanwhile, the P2ABSA/TiO_2 nanocomposites showed excellent photocatalytic stability, which was dependent on the structural stability. A photocatalytic activity enhanced mechanism has been proposed, accounting for the photosensitization effect and synergetic effect of TiO_2 with P2ABSA. Mass spectroscopy (MS) analysis showed that there were two possible degradation pathways for MB, *via* degradation of the chromophoric group or degradation of the auxochrome group.

2. Experimental

2.1 Reagents and materials

P25 TiO_2 with a specific surface area of 57.369 $m^2\ g^{-1}$ was purchased from Degussa. 2-Aminobenzene sulfonic acid (2ABSA) was purchased from Beijing J&K Scientific Ltd. Ammonium persulfate (APS) was purchased from Tianjin Kermel Chemical Reagent Co., Ltd. Ethanol was purchased from Tianjin Fuyu Fine Chemical Co., Ltd. Hydrochloric acid was purchased from Sinopharm Chemical Reagent Co., Ltd. Methylene blue (MB) was purchased from Tianjin Guangcheng Chemical Reagent Co., Ltd. All chemicals were of analytical grade and used without further purification. Deionized water was used to prepare all solutions.

2.2 Preparation of P2ABSA/TiO_2 nanocomposites

A typical synthesis of P2ABSA/TiO_2 nanocomposites is described below.[24]

An appropriate amount of 2ABSA was dissolved in hydrochloric acid solution (90 mL, 1.2 mol L^{-1}) followed by the addition of TiO_2 (0.512 g). The solution was ultrasonicated for 15 min to ensure uniform mixing. After dissolution, the solution was labeled as A. An appropriate amount of APS was dissolved in hydrochloric acid solution (30 mL, 1.2 mol L^{-1}), and this solution was labeled as B. Solution A was transferred to a 250 mL round-bottom flask and the solution was stirred using a magnetic stirrer. Solution B was transferred to a 100 mL constant-pressure funnel, and then solution A was added dropwise at approximately 1 drop/s with stirring. The reaction was continued for 24 h at 25 °C. The final products were filtered, washed with deionized water and ethanol, and dried at 80 °C for several hours in a vacuum oven. In the experiment, different initial [2ABSA]/[TiO_2] molar ratios (from 1 : 6 to 4 : 1) were employed to obtain TiO_2 nanocomposites deposited by P2ABSA with an initial [APS]/[2ABSA] molar ratio of 1/1 and HCl concentration of 1.2 mol L^{-1}. These nanocomposites are referred to as P/T(1/6), P/T(1/5), P/T(1/4), P/T(1/2), P/T(1/1), P/T(2/1) P/T(3/1), and P/T(4/1), respectively. To confirm the effect of P2ABAS on the nanocomposites, the P25 TiO_2 nanocomposites were treated using the same procedure without the addition of 2ABSA.

P2ABSA was also prepared *via in situ* oxidative polymerization using the same procedure as above, but without TiO_2 addition.

2.3 Characterization

SEM images were obtained on a JSM-6700F cold field emission scanning electron microscope and used to determine the morphology and aggregation of the photocatalyst.

XRD patterns were recorded on a Bruker D8 Advance X-ray diffractometer with Cu Kα radiation ($\lambda = 1.5418$ Å).

TEM images were obtained on a JEM-2100 transmission electron microscopy operating at 125 kV and used to determine the grain sizes of TiO_2 and P2ABSA/TiO_2.

XPS measurements were performed using a Thermo ESCALAB 250Xi system with an Al Kα X-ray source. All binding energies were referenced to the C1s peak at 284.8 eV, which corresponds to surface adventitious carbon.

UV-vis DRS was performed on a UV-2550PC ultraviolet and visible spectrophotometer with $BaSO_4$ as the background, ranging from 200 to 800 nm.

The photocurrent test was performed on a CHI660D VersaSTAT. TiO_2 and P2ABSA/TiO_2 nanocomposites were deposited as a film on a 1 cm × 1 cm indium-tin-oxide conducting glass to

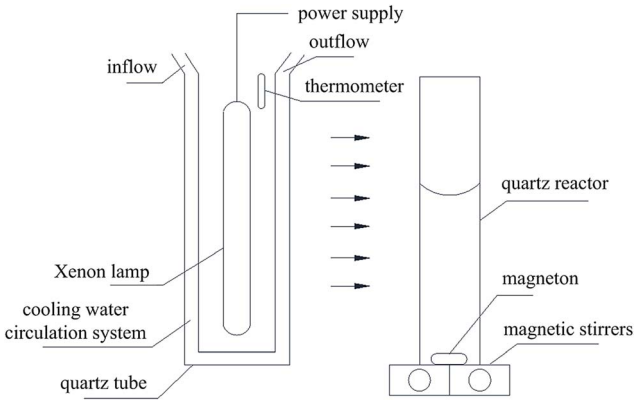

Fig. 1 Schematic diagram of the photocatalysis reactor (illumination intensities of visible light and UV were 28.5–30.0 mW cm^{-2} and 0.165–0.170 mW cm^{-2}, respectively, and the distance between the light source and quartz reactor was 7 cm).

obtain the working electrode. The saturated calomel electrode and a Pt electrode served as the reference and counter electrodes, respectively. The electrolyte was 0.1 mol L^{-1} $NaClO_4$ solution.

2.4 Photocatalytic activity test

Photocatalytic activities of samples were evaluated based on MB degradation in an aqueous solution under irradiation from a 1000 W xenon lamp (BL-GHX-V photochemical reactions instrument, Fig. 1). Aqueous suspensions of MB (30 mL, 40 mg L^{-1}) were placed in a quartz tube, and TiO_2 or P2ABSA/TiO_2 nanocomposites (30 mg) were added. Prior to irradiation, the suspensions were magnetically stirred in the dark for 1 h. The suspensions were maintained under constant air-equilibrated conditions before and during illumination. At certain time intervals, 1 mL aliquots were removed and centrifuged to remove any particles. The filtrates were then analyzed by recording variations in the maximum absorption band (664 nm for MB) using the UV-2550PC UV-vis spectrophotometer. This process was repeated five times to investigate the stability of the nanocomposites.

3. Results and discussion

3.1 Physicochemical properties of TiO_2 and P2ABSA/TiO_2 nanocomposites

3.1.1 TEM. TEM images of TiO_2 and P2ABSA/TiO_2 nanoparticles are shown in Fig. 2a and b. The grain sizes of both modified and P25 TiO_2 were monodisperse and approximately 30–50 nm in size, indicating that the presence of P2ABSA did not significantly affect the TiO_2 grain size. The aggregation of both types of particles was caused by a high surface energy. However, agglomeration of the modified nanocomposite was lower than that of the P25 particles. The TiO_2 nanoparticles deposited with P2ABSA avoided agglomeration because the positively charged deposited groups repelled each other.[25]

3.1.2 XRD. The XRD patterns of TiO_2 and P2ABSA/TiO_2 are shown in Fig. 3. The peaks at 2θ values of 25.4°, 37.9°, 48.2°, 54.0°, 62.8°, and 68.7° were attributed to the (101), (004), (200), (105), (204), and (116) faces of anatase TiO_2, respectively.[26] Furthermore, the peaks at 2θ values of 27.5° and 77.3° were assigned to the (110) and (215) faces of rutile TiO_2, respectively.[27] These results indicated that two phases were present in the patterns. Moreover, the P2ABSA/TiO_2 nanocomposites did not cause any change in the peak positions and shapes compared with those observed for TiO_2, indicating that the presence of P2ABSA did not affect the TiO_2 lattice structure.

3.1.3 XPS. XPS is an important tool for studying the electronic structure of condensed matter and is widely used in quantitative surface analysis. According to the XPS survey spectra of TiO_2 and P2ABSA/TiO_2 (Fig. 4a and b), the presence of Ti and O in TiO_2 was confirmed by the two peaks at binding energies of 458.5 and 529.8 eV.[28] Furthermore, the presence of C, O, Ti, N, and S in P2ABSA/TiO_2 were confirmed by the five peaks at binding energies of 284.8, 529.8, 458.5, 400.3 and 168.7 eV, which were related to C1s, O1s, Ti2p, N1s, and S2p, respectively.[29] The atomic abundances of C, O, Ti, N, and S were 14.1%, 59.06%, 25.11%, 0.95%, and 0.78%, respectively, suggesting that P2ABSA existed on the TiO_2 surface.

3.1.4 UV-vis DRS. UV-vis DRS spectra of TiO_2, P2ABSA, and P2ABSA/TiO_2 nanocomposites are shown in Fig. 5a. P2ABSA had a high absorption in both the UV and visible light regions. In comparison with TiO_2, the absorption of P2ABSA/TiO_2 had been extended throughout the visible light range, but had decreased in the UV range. This result indicated that our method was effective for extending the absorption of TiO_2 to the visible light region. As shown in Fig. 5b, the band gap energies (E_g) of modified and P25 TiO_2, obtained from the wavelength values corresponding to the intersection point of the vertical and horizontal portions of the spectra using $hc/\lambda = E_g$, where E_g is the band gap energy, h is Planck's constant, c is the speed of light (m s^{-1}), and λ is the wavelength (nm), were determined as

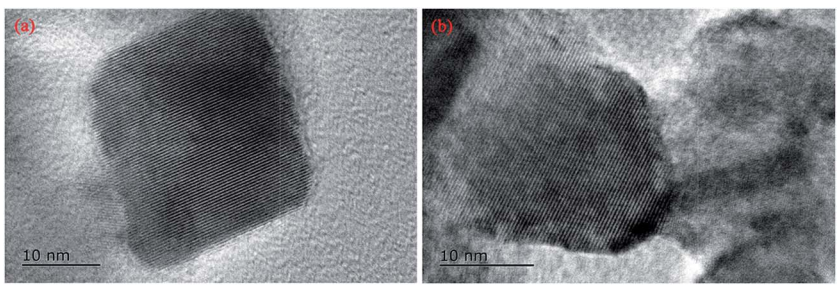

Fig. 2 TEM images of (a) TiO_2 and (b) P/T(2/1) nanocomposites.

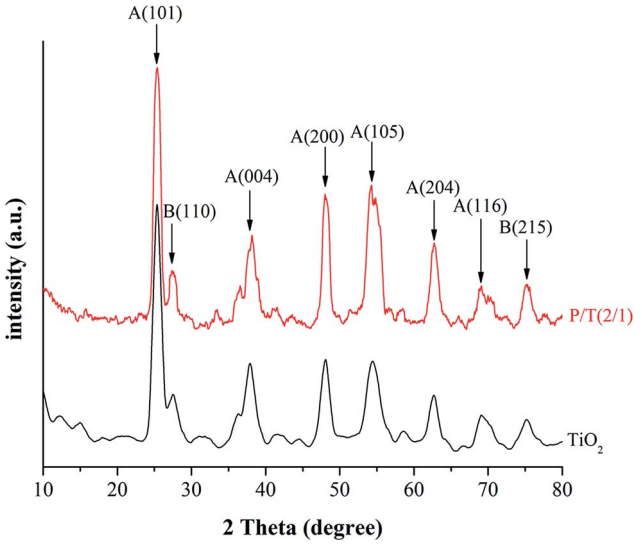

Fig. 3 XRD patterns of TiO_2 and P/T(2/1) nanocomposites (A and B represent anatase and rutile TiO_2, respectively).

2.70 eV and 3.11 eV, respectively.[30] Therefore, the P2ABSA/TiO_2 nanocomposites could be excited to produce more electron–hole pairs under visible light illumination, which might result in higher photocatalytic activities.

3.1.5 Photocurrent test. As shown in Fig. 6, the photocurrent density of TiO_2 was low (approx.14 μA cm^{-2}) because TiO_2 is a semiconductor with a wide band gap. However, the photocurrent density of the P2ABSA/TiO_2 nanocomposite was approx. 28 μA cm^{-2}, twice that of TiO_2. These results confirmed that the presence of P2ABSA improved the photocurrent density of the P2ABSA/TiO_2 photocatalyst. P2ABSA had excellent electrical conductivity to transfer free electrons from the valence band (VB) to the conduction band (CB), demonstrating that P2ABSA/TiO_2 had a higher photocurrent density and photocatalytic performance than TiO_2. Similar results were also obtained by Liao *et al.*[31] for a photonic crystal coupled TiO_2/polymer hybrid for efficient photocatalysis under visible light irradiation. These results proved that the combination of TiO_2 and P2ABSA was an effective way to improve photocatalytic activity.

3.2 Photocatalytic activity and stability

3.2.1 Photocatalytic activity of P2ABSA/TiO_2 nanocomposites. Photocatalytic activity tests were performed by degrading MB in an aqueous solution under irradiation with a 1000 W xenon lamp. MB has a maximum absorption at 664 nm. Fig. 7a shows the degradation of MB in the presence of TiO_2 and P2ABSA/TiO_2 with different initial ratios of 2ABSA to TiO_2. As shown in Fig. 7b, the kinetics plots show an apparent

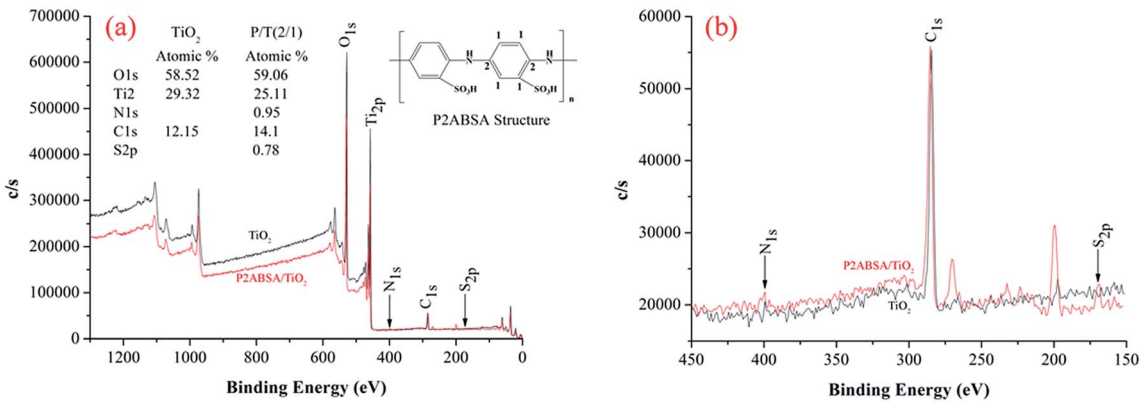

Fig. 4 (a) XPS spectra of TiO_2 and P/T(2/1) nanocomposites and (b) peaks of N1s and S2p for P/T(2/1) nanocomposite.

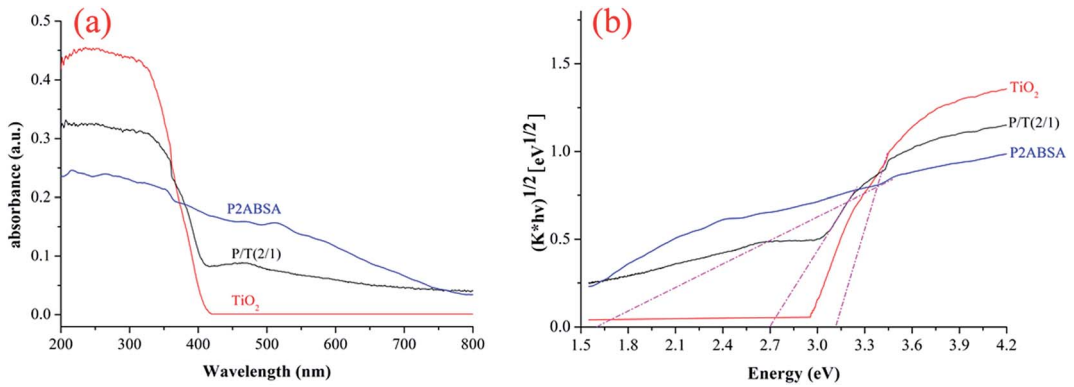

Fig. 5 (a) UV-vis DRS and (b) E_g of P2ABSA, TiO_2, and P/T(2/1) nanocomposites.

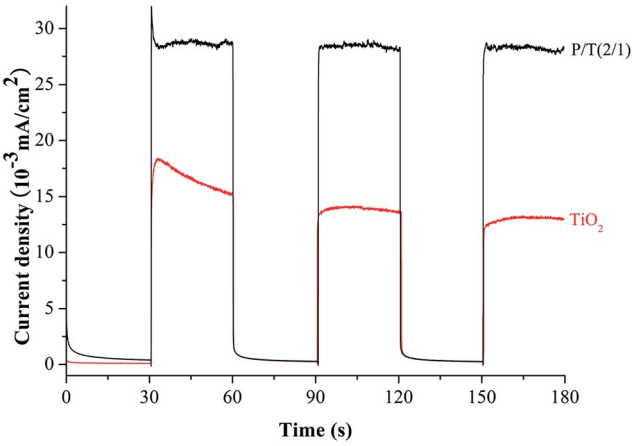

Fig. 6 Photocurrent test of TiO_2 and P/T(2/1) nanocomposites.

first-order linear form ($-\ln(C/C_0) = k_{app}t$).[32] The activities of TiO_2 and the modified photocatalysts were evaluated by comparing the apparent first-order rate constants (k_{app}) listed in Table 1. TiO_2 and P/T(2/1) nanocomposites exhibited apparent rate constants of 0.0021 min^{-1} and 0.0138 min^{-1}, respectively, showing that P/T(2/1) enhanced the photocatalytic activity. The MB degradation rate exhibited an "up-down-up-down" trend as a function of the initial molar ratios of 2ABSA to TiO_2, which ranged from 1 : 6 to 4 : 1.

The initial [2ABSA]/[TiO_2] molar ratios clearly had a significant influence on the activity of P2ABSA/TiO_2 nanocomposites in the degradation of MB, and the optimal initial [2ABSA]/[TiO_2] molar ratio was 2 : 1. The photocatalytic activity of P2ABSA/TiO_2 nanocomposites with different initial [2ABSA]/[TiO_2] molar ratios was influenced by the thickness of P2ABSA on the TiO_2 surface.[33] When the molar ratio of 2ABSA to TiO_2 was low, increasing the molar ratio increased the thickness of deposited P2ABSA on the TiO_2 surface, such that the produced electron–hole pairs accumulated under irradiation, enhancing the photocatalytic performance. However, as the molar ratio of 2ABSA to TiO_2 continued increasing, the thickness of deposited P2ABSA on the TiO_2 surface became too thick to influence the transmission of the produced electrons, resulting in the photocatalytic performance of P2ABSA/TiO_2 nanocomposites decreasing.

3.2.2 Photocatalytic stability of P2ABSA/TiO_2 nanocomposites. Experiments were performed to confirm the photocatalytic stability of the P/T(2/1) nanocomposite, which exhibited good photocatalytic stability under irradiation conditions and maintained its photocatalytic activity after five cycles (Fig. 8a). As explained by Li Xueyan and co-authors[25] in the degradation of phenol with a PANI/TiO_2 nanocomposite, a slight decrease in the photocatalytic activity in each successive cycle was due to the slight aggregation of nanocomposites during the photocatalytic process (Fig. 8b and c). FT-IR spectra of the P/T(2/1) nanocomposite before and after the reaction were used to explain the stability of the P/T(2/1) nanocomposite (Fig. 8d). The shapes of the FT-IR spectra before and after photocatalysis were similar, indicating that the structure of the P/T(2/1) nanocomposite did not change during the photocatalytic process. P2ABSA is very stable and is not chemically transformed into other organic compounds, meaning that the stability of photocatalytic activity was dependent on the structural stability.

3.3 Photocatalytic activity enhanced mechanism

Although the photocatalytic activity of the photocatalyst was influenced by many factors, two key factors were identified from

Table 1 Apparent first-order rate constants (k_{app}) of MB degradation and linear regression coefficients from a plot of $-\ln(C/C_0) = k_{app}t$

Photocatalysts	$-\ln(C/C_0) = k_{app}t$	k_{app} (min^{-1})	R^2
TiO_2	$-\ln(C/C_0) = 0.0021t$	0.0021	0.9851
P/T(1/6)	$-\ln(C/C_0) = 0.0073t$	0.0073	0.9963
P/T(1/5)	$-\ln(C/C_0) = 0.0081t$	0.0081	0.9917
P/T(1/4)	$-\ln(C/C_0) = 0.0092t$	0.0092	0.9964
P/T(1/2)	$-\ln(C/C_0) = 0.0126t$	0.0126	0.9980
P/T(1/1)	$-\ln(C/C_0) = 0.0105t$	0.0105	0.9995
P/T(2/1)	$-\ln(C/C_0) = 0.0138t$	0.0138	0.9987
P/T(3/1)	$-\ln(C/C_0) = 0.0073t$	0.0073	0.9979
P/T(4/1)	$-\ln(C/C_0) = 0.0029t$	0.0029	0.9976

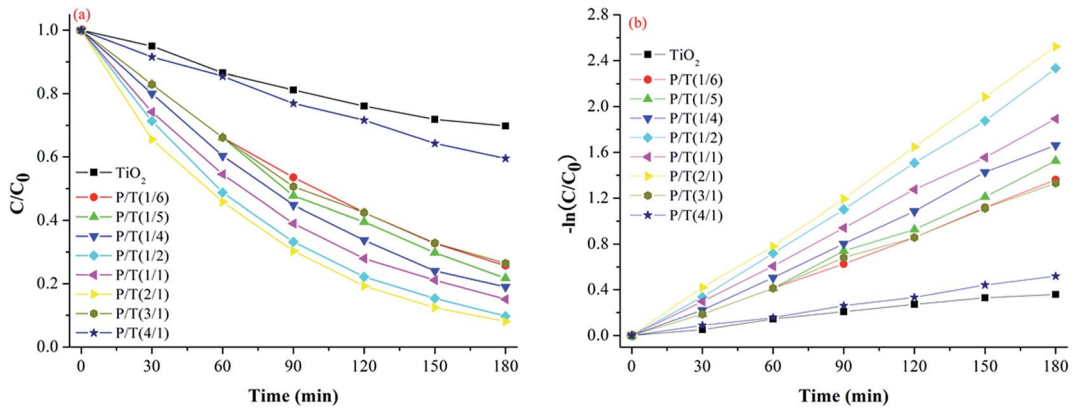

Fig. 7 (a) Photocatalytic degradation and (b) apparent first-order linear transforms, $-\ln(C/C_0)$, of MB in the presence of TiO_2 and P/T(2/1) nanocomposites.

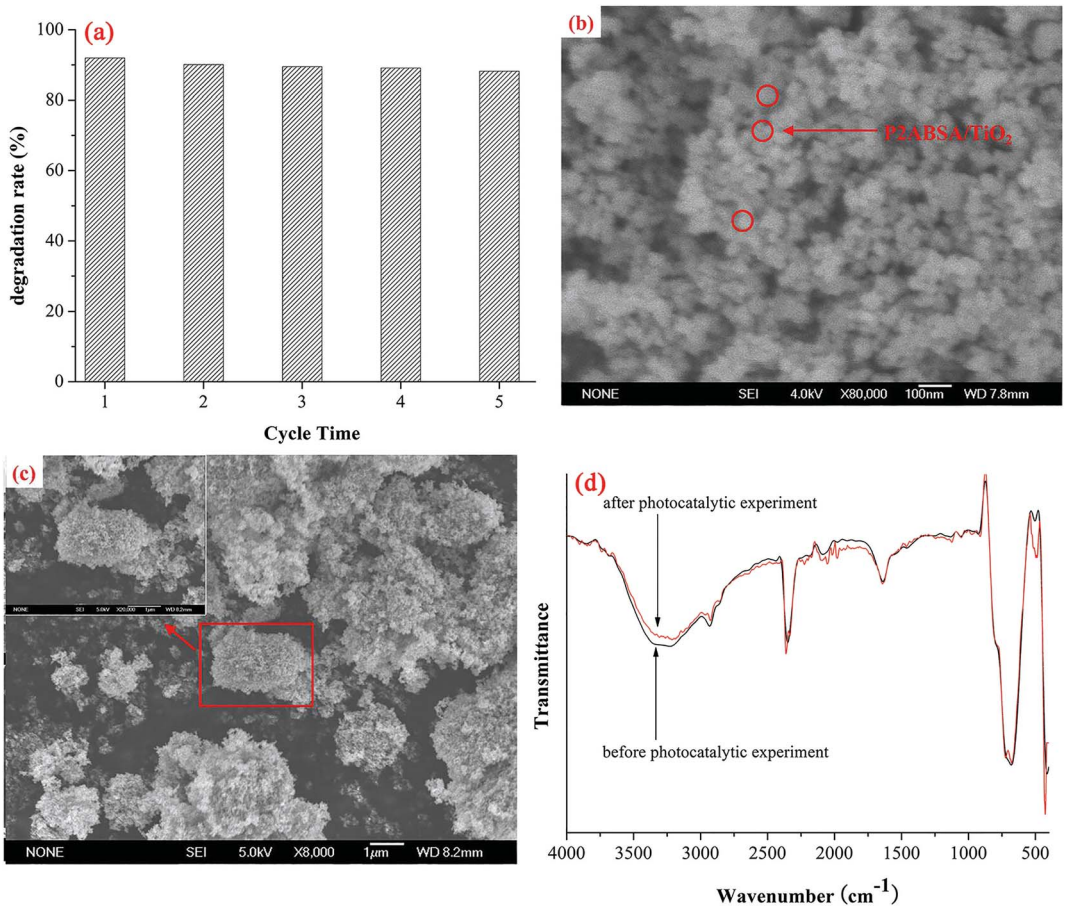

Fig. 8 (a) Photocatalytic degradation rate of MB using P/T(2/1) nanocomposite with different recycling times, (b) SEM image of P/T(2/1) nanocomposite before photocatalytic degradation, (c) SEM image of P/T(2/1) nanocomposite after photocatalytic degradation with slight aggregation, and (d) FT-IR spectra of P/T(2/1) before and after photocatalytic degradation.

the photocatalytic mechanism. In the primary reaction process, TiO_2 is excited under light irradiation to generate electron–hole pairs. In the secondary reaction process, ROS are produced to degrade the organic pollutant. Therefore, the two key factors in the photocatalytic activity were solar absorption and charge separation.

For P2ABSA/TiO_2, as P2ABSA is a photosensitizer, based on its narrow band gap, P2ABSA-modified TiO_2 inserts the energy level of P2ABSA into the energy level of TiO_2, enhancing its response to visible light. However, the synergetic effect resulting from the good match between the energy levels of TiO_2 and P2ABSA causes P2ABSA/TiO_2 to hinder the recombination of holes and electrons to generate more ROS to degrade MB. Therefore, the mechanism for enhanced photocatalytic activity is based on photosensitization and synergetic effects.

3.3.1 Photosensitization effect that enhances visible light. For a crystalline semiconductor, optical absorption near the band edge can be expressed using the Kubelka–Munk function:[34]

$$F(R)E = A(E - E_g)^{n/2} \quad (1)$$

where $F(R)$, E, A, n, and E_g are the diffuse absorption coefficient, photon energy, proportionality constant, an integer ($n = 1, 2, 4, 6$), and band gap, respectively. For TiO_2, P2ABSA, and P2ABSA/TiO_2, the relationship between the diffuse absorption coefficient and the band gap energy is described by eqn (2):

$$(F(R)E)^{1/2} = A(E - E_g) \quad (2)$$

In eqn (2), $(F(R)E)^{1/2}$ has a linear relationship with E. The n value for the samples was determined to be 4, indicating that the optical transitions of the crystal were indirectly forbidden.[35,36] Fig. 5b shows the optical band gaps (E_g) of TiO_2, P2ABSA, and P2ABSA/TiO_2. The band gap energies for TiO_2, P2ABSA, and P2ABSA/TiO_2 were determined to be 3.11, 1.61, and 2.70 eV, respectively, indicating that P2ABSA-modified TiO_2 was a better photocatalyst than unmodified TiO_2 owing to P2ABSA acting as a photosensitizer.

The π–π* absorption of P2ABSA is low because the benzene rings are conjugated through an imine linkage and the sulfonyl group is electron-withdrawing. The experimental absorption spectrum for P2ABSA indicated a band gap of 1.61 eV, which was interpreted as excitation to the polaron band. P2ABSA is an

efficient electron donor and hole transporter upon light excitation. In the P2ABSA and TiO_2 combined system, the response to light ranged from 398 nm (UV) to 459 nm (visible light). Therefore, because of the photosensitization effect of P2ABSA, the P2ABSA/TiO_2 nanocomposites exhibited stronger responses to visible light, and the photocatalytic activity of P2ABSA-modified TiO_2 was enhanced by the improved response to visible light.

3.3.2 Synergetic effect that enhances ROS generation. TiO_2 and P2ABSA in P2ABSA-modified TiO_2 have a synergetic effect on the photocatalytic degradation of MB due to their well-matched energy levels, with the optimum synergetic effect observed for P/T(2/1). The energy levels of TiO_2 and P2ABSA matched with $E_{(LUMO)} > E_{(CB)} > E_{(HOMO)} > E_{(VB)}$ (where CB represents conduction band, VB represents valence band, LUMO represents lowest unoccupied molecular orbital, and HOMO represents highest occupied molecular orbital). Under irradiation, electrons are excited from the HOMO to the LUMO to the CB. Furthermore, the holes transfer from the VB to the HOMO owing to P2ABSA acting as a hole transporter. Therefore, electrons and holes gather in the CB of TiO_2 and HOMO of P2ABSA, respectively. Meanwhile, the electrons react with O_2 to produce $^{\bullet}O_2^-$, and the holes react with H_2O or OH^- to produce $^{\bullet}OH$. These generated ROS ($^{\bullet}O_2^-$ and $^{\bullet}OH$) are responsible for MB degradation. This Z-scheme photocatalytic mechanism is beneficial for enhancing the generation of ROS owing to an increase in the separation efficiency between holes and electrons.[37,38]

The synergetic factor (f) was then calculated using the apparent first-order kinetic expression:[39]

$$-\frac{dR}{dt} = k_{C/T}[C_t] = k_C[C_t] + k_T[C_t] + k_{C-T}[C_t] \quad (3)$$

where $k_{C/T}$ is the first-order rate constant of P2ABSA/TiO_2, k_C is the first-order rate constant of P2ABSA, k_T is the first-order rate constant of TiO_2, and $[C_t]$ is the concentration of MB. Therefore, the photocatalytic degradation of MB is influenced by the degradation of TiO_2 and P2ABSA and the synergy between P2ABSA and TiO_2. The synergetic factor can be calculated using the following equation:

$$f = \frac{k_{C/T}}{k_C + k_T} \quad (4)$$

Based on the mass of TiO_2 being much greater than that of P2ABSA (XPS results in Fig. 4a and b), and P2ABSA being used as a modifier with no obvious photocatalytic activity ($k_C \approx 0$), f was calculated as follows:

$$f = \frac{k_{C/T}}{k_T} \quad (5)$$

Based on the apparent first-order kinetic constants for MB degradation in Table 1, the synergetic factors of the P2ABSA/TiO_2 nanocomposites were 3.48 for P/T(1/6), 3.86 for P/T(1/5), 4.38 for P/T(1/4), 6 for P/T(1/2), 5 for P/T(1/1), 6.57 for P/T(2/1), 3.48 for P/T(3/1), and 1.38 for P/T(4/1). Therefore, the photocatalytic activities of P2ABSA-modified TiO_2 were enhanced by increased ROS generation.

3.4 Intermediate products and degradation pathways of MB

Using UHR-TOF-MS (Bruker Daltonic Inc., USA), the intermediate products of MB degradation were identified. MB exhibits one main band in the visible region with a maximum absorption at 664 nm and a small shoulder at 610 nm owing to the dye dimer. Furthermore, two bands were present in the ultraviolet region at 246 nm and 292 nm. The color of MB is dependent on its chromophoric (N–S conjugated system on central aromatic heterocycle) and auxochrome groups (N-containing groups with lone pair electrons on benzene ring).[40] During the photocatalytic process, the removal of MB includes not only adsorption, but also degradation using the P2ABSA-modified TiO_2 nanocomposites. Based on the coloring mechanism, decolorizing mechanism, and the intermediate products, we proposed two possible photocatalytic degradation pathways for MB.

3.4.1 First degradation pathway: chromophoric group degradation. During electronic reorganization, sulfhydryl (C–S^+=C) is converted to a sulfoxide (C–S(=O)–C), and the central aromatic heterocycle opens. Electrophilic attack by $^{\bullet}OH$ at the free doublet of the S heteroatom changes its oxidation from −2 to 0. However, the conversion from C–$S^+$$^{\bullet}$C to C–S($^{\bullet}$O)–C requires conservation of the double bond conjugation, which induces opening of the central aromatic ring containing both heteroatoms (S and N). The H atoms necessary for C–H and N–H bond formation may originate from proton reduction caused by photogenerated electrons. The intermediate products of MB degradation included 2-amino-5-(*N*-methyl formamide)benzene sulfonic acid (m/z = 230), 2-amino-5-(methyl amino)-hydroxybenzene sulfonic acid (m/z = 218), benzenesulfonic acid (m/z = 158), and phenol (m/z = 94). Degradation of the chromophoric group is shown in Fig. 9.

3.4.2 Second degradation pathway: auxochrome group degradation. Further analysis of product formation was performed based on mass spectroscopy (MS) studies of the intermediate products from degradation. We identified various intermediate products, including azure A (m/z = 270), azure B (m/z = 256), azure C (m/z = 242), and thionin (m/z = 228), that were formed *via* demethylation cleavage during the photocatalytic degradation. Demethylation during the degradation of MB is shown in Fig. 10.

All the intermediate products formed during MB photocatalytic degradation were identified from mass spectra, as shown in Fig. 11.

3.5 Photocatalytic mechanism of P2ABSA/TiO_2 nanocomposites

The basic mechanism of P2ABSA/TiO_2 nanocomposites was well established. TiO_2 nanocomposites are irradiated with UV light to generate electron–hole pairs, which can react with water to yield hydroxyl and superoxide radicals, which oxidize and mineralize the organic molecules. However, the band gap of

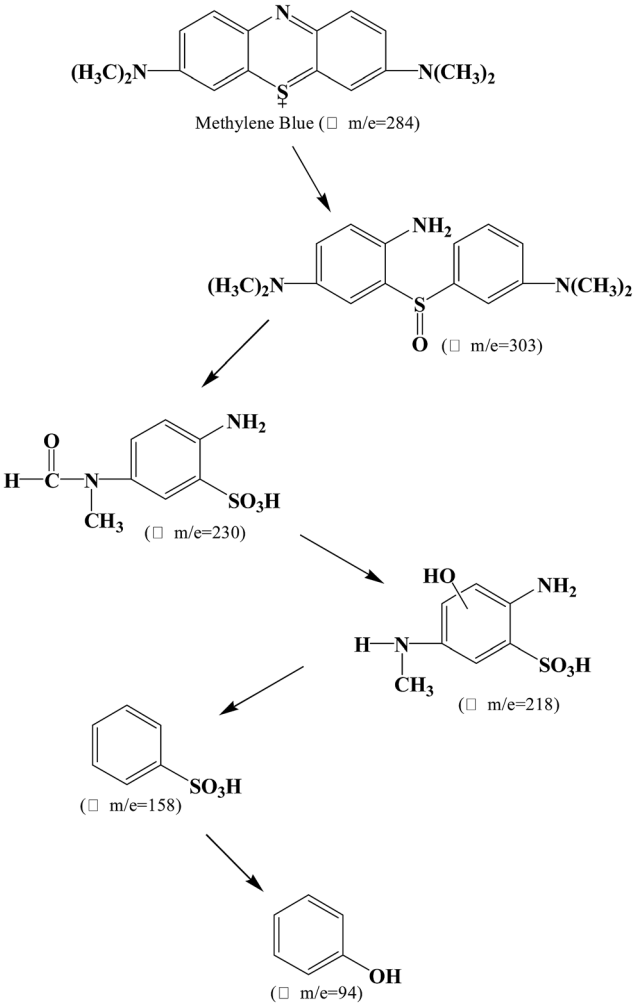

Fig. 9 First degradation pathway of MB: chromophoric group degradation.

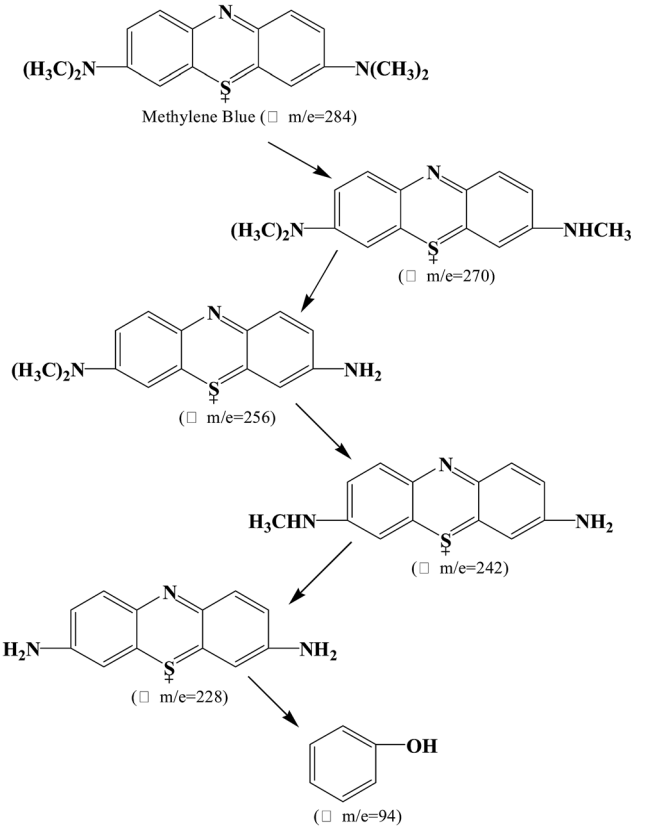

Fig. 10 Second degradation pathway of MB: auxochrome group degradation.

TiO_2 is 3.11 eV, meaning that only UV light can excite the TiO_2 nanocomposites to generate electron–hole pairs. One solution to overcome this shortcoming was to use a dye with a narrow band gap as a sensitizer to enhance the response of TiO_2 to visible light. P2ABSA has a band gap of 1.61 eV, which is narrower than that of TiO_2 (3.2 eV), showing strong absorption in the region of visible light. Therefore, P2ABSA can function as a photosensitizer for TiO_2.

When P2ABSA/TiO_2 nanocomposites are illuminated under visible light, both TiO_2 and P2ABSA absorb photons at their interface, where charge separation then occurs. This happens because the CB of TiO_2 and the LUMO of P2ABSA are well matched for charge transfer. Electrons generated by conducting P2ABSA can be transferred to the conduction band of TiO_2, enhancing charge separation and promoting the photocatalytic ability of the photocatalyst.

The synergetic effect between P2ABSA and TiO_2 on the photocatalytic degradation of MB clearly existed in all the P2ABSA/TiO_2 nanocomposites. An optimum synergetic effect was found in P/T(2/1). The effect of P2ABSA on the activity of the nanocomposites can be explained by its action as photosensitizer (Scheme 1). Doped P2ABSA semiconductive material can absorb visible light irradiation and transfer photogenerated electrons into the CB of TiO_2. Simultaneously, a positively charged hole can be formed by the electron, transferring from the VB of TiO_2 to the HOMO of P2ABSA. This electron transfer between P2ABSA and the TiO_2 semiconductor, and the enhanced photocatalytic activity of the composites, have been experimentally observed in other systems.[41,42] The free electrons reacted with O_2 to produce superoxide radicals ($^{\bullet}O_2^-$), and the holes (h^+) reacted with OH^- and H_2O to produce hydroxyl radicals ($^{\bullet}OH$), which are responsible for MB degradation.[43]

The photocatalytic mechanism of P2ABSA/TiO_2 nanocomposites can be expressed as follows:

$$\text{P2ABSA/TiO}_2 + h\nu \rightarrow \text{P2ABSA}^+/\text{TiO}_2 + \text{e}^- \quad (6)$$

$$\text{e}^- + \text{O}_2 \rightarrow {}^{\bullet}\text{O}_2^- \quad (7)$$

$$\text{P2ABSA}^+/\text{TiO}_2 \rightarrow \text{P2ABSA/TiO}_2 + \text{h}^+ \quad (8)$$

$$\text{h}^+ + \text{H}_2\text{O/OH}^- \rightarrow {}^{\bullet}\text{OH} \quad (9)$$

$$\text{MB} + \text{ROS} \rightarrow \text{CO}_2 + \text{H}_2\text{O} \quad (10)$$

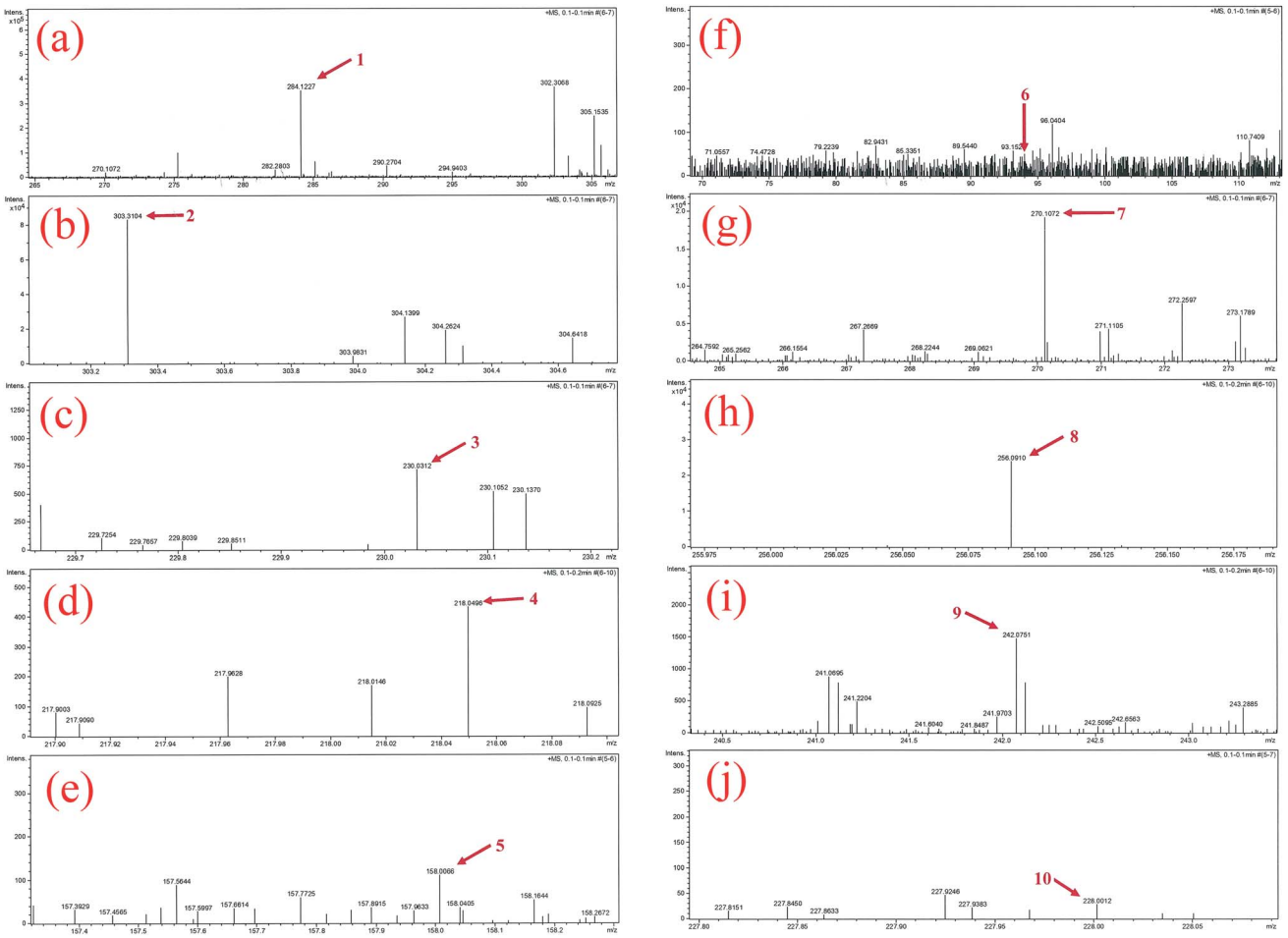

Fig. 11 MS results for MB during the photocatalytic degradation process (a and f represent original MB ① and phenol ⑥, respectively; b, c, d, and e represent intermediate products ②, ③, ④, and ⑤ in the first degradation pathway of MB, respectively; g, h, i and j represent intermediate products ⑦, ⑧, ⑨, and ⑩ in the second degradation pathway of MB, respectively).

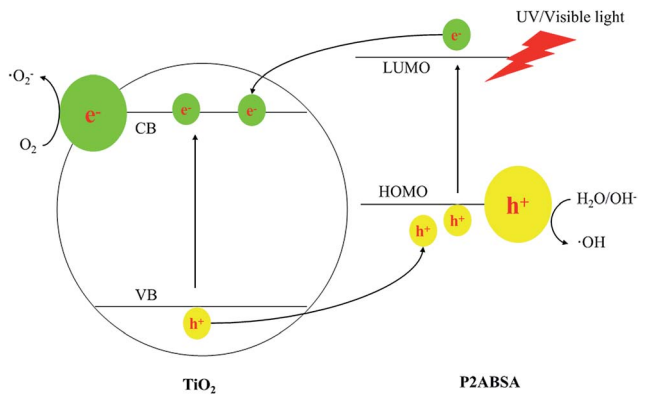

Scheme 1 Photocatalytic mechanism of P2ABSA/TiO_2 nanocomposites.

4. Conclusions

In this study, P2ABSA/TiO_2 nanocomposites were synthesized using an *in situ* oxidative polymerization method. The modified photocatalysts were characterized by SEM, XRD, TEM, XPS, UV-vis DRS, and a photocurrent test. The results indicated that P2ABSA was present on the TiO_2 surface and did not impact the lattice structure and grain size of TiO_2. The presence of P2ABSA enhanced the visible light response and photoelectric performance. The photocatalytic degradation of MB was chosen as a model reaction to evaluate the photocatalytic activities of TiO_2 and P2ABSA/TiO_2 nanocomposites, with results indicating that P2ABSA/TiO_2 nanocomposites exhibited the higher activity. The apparent first-order rate constant, k_{app}, of P/T(2/1) was 0.0138 min^{-1}, which was six times higher than that of TiO_2 (0.0021 min^{-1}). Meanwhile, the P2ABSA/TiO_2 nanocomposites showed excellent photocatalytic stability, which was dependent on the structural stability. A photocatalytic activity enhanced mechanism has been proposed, accounting for the photosensitization effect and synergetic effect of TiO_2 with P2ABSA. Based on the analysis of mass spectra, two possible degradation pathways for MB degradation were identified, *via* the chromophoric group or the auxochrome group. Our results provide valuable insight into the design of polymer-modified semiconductors with excellent performance and provide a foundation for future industrial applications.

Acknowledgements

This work was supported by the 973 Program (2013CB 933800), the National Natural Science Foundation of China (41672340, 21507074, 21405096, 21301110), and Shandong Provincial Natural Science Foundation, China (BS2014NJ008).

References

1 A. Fujishima and K. Honda, *Nature*, 1972, **238**, 37–38.
2 K. Nakata and A. Fujishima, *J. Photochem. Photobiol., C*, 2012, **13**, 169–189.
3 M. Pelaez, N. T. Nolan, S. C. Pillai, M. K. Seery, P. Falaras, A. G. Kontos, P. S. M. Dunlop, J. W. J. Hamilton, J. A. Byrne, K. O'Shea, M. H. Entezari and D. D. Dionysiou, *Appl. Catal., B*, 2012, **125**, 331–349.
4 W. Zhang, B. P. Jia, Q. Z. Wang and D. Dionysiou, *J. Nanopart. Res.*, 2015, **17**, 1–12.
5 X. F. Shi, N. Li, K. Zhao, G. W. Cui, Y. Q. Zhao, M. Y. Ma, K. H. Xu, P. Li, Y. B. Dong and B. Tang, *Appl. Catal., B*, 2013, **136**, 334–340.
6 D. H. Kuo, W. T. Hsu and Y. Y. Yang, *Appl. Catal., B*, 2016, **184**, 191–200.
7 H. Park, Y. Park, W. Kim and W. Choi, *J. Photochem. Photobiol., C*, 2013, **15**, 1–20.
8 K. R. Reddy, M. Hassan and V. G. Gomes, *Appl. Catal., A*, 2015, **489**, 1–16.
9 S. Seema, M. Hari and K. S. Pramod, *Appl. Catal., A*, 2013, **462–463**, 178–195.
10 P. Muthirulan, C. K. N. Devi and M. M. Sundaram, *J. Environ. Chem. Eng.*, 2013, **1**, 620–627.
11 H. Zhang, R. L. Zong, J. C. Zhao and Y. F. Zhu, *Environ. Sci. Technol.*, 2008, **42**, 3803–3807.
12 Z. Y. Zhu, F. L. Wang, F. M. Wang and L. L. Xi, *J. Electroanal. Chem.*, 2013, **708**, 13–19.
13 Y. W. Hu, T. Yang, X. X. Wang and K. Jiao, *Chem.–Eur. J.*, 2010, **16**, 1992–1999.
14 Y. B. Liu, G. Q. Zhu, J. Z. Gao, R. L. Zhu, M. Hojamberdiev, C. H. Wang, X. M. Wei and P. Liu, *Appl. Catal., B*, 2017, **205**, 421–432.
15 X. F. Shi, X. Y. Xia, G. W. Cui, N. Deng, Y. Q. Zhao, L. H. Zhuo and B. Tang, *Appl. Catal., B*, 2015, **163**, 123–128.
16 H. Lachheb, E. Puzenat, A. Houas, M. Ksibi, E. Elaloui, C. Guillard and J. M. Herrmann, *Appl. Catal., B*, 2002, **39**, 75–90.
17 J. F. Luan, X. P. Hao, S. R. Zheng, G. Y. Luan and X. S. Wu, *J. Mater. Sci.*, 2006, **41**, 8001–8012.
18 Y. H. Zhang, Z. R. Tang, X. Z. Fu and Y. J. Xu, *ACS Nano*, 2010, **4**, 7303–7314.
19 A. Houas, H. Lachheb, M. Ksibi, E. Elaloui, C. Guillard and J. M. Herrmann, *Appl. Catal., B*, 2001, **31**, 145–157.
20 M. A. Rauf, M. A. Meetani, A. Khaleel and A. Ahmed, *Chem. Eng. J.*, 2010, **157**, 373–378.
21 L. C. Zhou, J. J. Ma, H. Zhang, Y. M. Shao and Y. F. Li, *Appl. Surf. Sci.*, 2015, **324**, 490–498.
22 C. S. Castro, M. C. Guerreiro, L. C. A. Oliveira, M. Goncalves, A. S. Anastacio and M. Nazzarro, *Appl. Catal., A*, 2009, **367**, 53–58.
23 J. J. Ma, L. C. Zhou, W. F. Dan, H. Zhang, Y. M. Shao, C. Bao and L. Y. Jing, *J. Colloid Interface Sci.*, 2015, **446**, 298–306.
24 M. Radoičić, Z. Šaponjić, I. A. Janković, G. Ćirić-Marjanović, S. P. Ahrenkiel and M. I. Čomor, *Appl. Catal., B*, 2013, **136**, 133–139.
25 X. Y. Li, D. S. Wang, G. X. Cheng, Q. Z. Luo, J. An and Y. Wang, *Appl. Catal., B*, 2008, **81**, 267–273.
26 Y. M. Lin, D. Z. Li, J. H. Hu, G. C. Xiao, J. X. Wang, W. J. Li and X. Z. Fu, *J. Phys. Chem. C*, 2012, **116**, 5764–5772.
27 Z. Zhao, X. Y. Zhang, G. Q. Zhang, Z. Y. Liu, D. Qu, X. Miao, P. Y. Feng and Z. C. Sun, *Nano Res.*, 2015, **8**, 4061–4071.
28 D. S. Wang, J. Zhang, Q. Z. Luo, X. Y. Li, Y. D. Duan and J. An, *J. Hazard. Mater.*, 2009, **169**, 546–550.
29 D. S. Wang, Y. H. Wang, X. Y. Li, Q. Z. Luo, J. An and J. X. Yue, *Catal. Commun.*, 2008, **9**, 1162–1166.
30 G. Z. Liao, S. Chen, X. Quan, Y. B. Zhang and H. M. Zhao, *Appl. Catal., B*, 2011, **102**, 126–131.
31 G. Z. Liao, S. Chen, X. Quan, H. Chen and Y. B. Zhang, *Environ. Sci. Technol.*, 2010, **44**, 3481–3485.
32 Y. F. Zhu and Y. Dan, *Sol. Energy Mater. Sol. Cells*, 2010, **94**, 1658–1664.
33 C. X. Yang, M. Zhang, W. P. Dong, G. W. Cui, Z. M. Ren and W. L. Wang, *PLoS One*, 2017, **12**, e0174104.
34 W. J. Li, D. Z. Li, Z. X. Chen, H. J. Huang, M. Sun, Y. H. He and X. Z. Fu, *J. Phys. Chem. C*, 2008, **112**, 14943–14947.
35 S. Debnath, N. Ballav, H. Nyoni, A. Maity and K. Pillay, *Appl. Catal., B*, 2015, **163**, 330–342.
36 S. Razak, M. A. Nawi and K. Haitham, *Appl. Surf. Sci.*, 2014, **319**, 90–98.
37 M. A. Salem, A. F. Al-Ghonemiy and A. B. Zaki, *Appl. Catal., B*, 2009, **91**, 59–66.
38 P. Zhou, J. G. Yu and M. Jaroniec, *Adv. Mater.*, 2014, **26**, 4920–4935.
39 A. P. Jia, G. S. Hu, L. Meng, Y. L. Xie, J. Q. Lu and M. F. Luo, *J. Catal.*, 2012, **289**, 199–209.
40 M. A. Sanromán, M. Pazos, M. T. Ricart and C. Cameselle, *Chemosphere*, 2004, **57**, 233–239.
41 H. C. Liang and X. Z. Li, *Appl. Catal., B*, 2009, **86**, 8–17.
42 W. Li, Y. Tian, C. H. Zhao, Q. Y. Zhang and W. C. Geng, *Chem. Eng. J.*, 2016, **303**, 282–291.
43 X. Ma and X. Y. Ni, *J. Mater. Sci.: Mater. Electron.*, 2015, **26**, 1129–1135.

